

pubs.acs.org/Macromolecules Article

# Shape Control over the Polymer Molecular Weight Distribution and Influence on Rheological Properties

Yanlin Shi, Sung-Po R. Chen, George Fragkiadakis, Daniele Parisi, Virgil Percec, Dimitris Vlassopoulos, and Michael J. Monteiro\*



Cite This: Macromolecules 2023, 56, 545-555



Log Mw

ABSTRACT: The shape, breadth, and average molecular weight of the overall molecular weight distribution (MWD) largely define polymer properties. In conventional free-radical polymerization, control over this distribution is through the many competing kinetic pathways dominated by radical termination events. "Living" radical polymerization mechanistically minimizes these termination events, providing a facile route to a desired Gaussian distribution with the distribution breadth dependent upon the activity of the catalyst or modulating agent. However, producing unusually shaped distributions can only be achieved through modeling of the complex polymerization kinetics and invoking feeding and other methods. Here, we construct square, slanted, and chair-like MWDs by blending two to four polymers made using a low-reactive RAFT agent with dispersities close to 2. The synthesis of these polymers, unlike that of polymers made with high-reactive RAFT agents, is simple, scalable, and importantly reproducible as the MWD is independent of conversion, making this polymerization method virtually and kinetically model-free. The blending method described here overcomes many of the difficulties in producing unusually shaped MWDs and allows control over the shape and breadth of the MWD. The concept further provides a general synthetic strategy for studying important structure—property relationships of polymers with desired processing and performance characteristics. This is demonstrated by measurement and modeling analysis of the linear viscoelastic properties of selected samples, which provides a way to tailor the properties of polymers by controlling the form of their MWD via blending. Unlike conventional approaches analyzing the effects of the MWD, its actual shape is considered and its effect on the properties is addressed.

#### INTRODUCTION

The average molecular weight, breadth, and shape of the molecular weight distribution (MWD) of a polymer determine its physical properties. 1-5 Controlling the MWD relies on an accurate understanding of the polymerization mechanism and knowledge of its associated kinetic parameters. In the case of conventional free-radical polymerization, accurate values and system dependencies for initiation, propagation, transfer, and termination allow the prediction of rates of polymerization and MWDs. Even with knowledge of these rate constants, control over the MWD using conventional free-radical polymerization is often difficult due to their dependence upon the polymerization system, including reactor type, monomer type, solvent, temperature, viscosity, and concentration. "Living" radical

polymerizations (LRPs) provide a polymerization method that significantly reduces these dependencies, especially transfer and termination, to generate polymers with excellent control over the MWD.<sup>7–10</sup> The main advantage of LRP is the production of narrow or close to monodisperse MWDs, although broader MWDs can be obtained by tuning the transfer agent or catalyst reactivity. The various LRP

Received: November 10, 2022 Revised: December 20, 2022 Published: December 30, 2022





(A) + 
$$Z = C_{4H_9} - S^* C_{tr,RAFT} > 10$$
; high transfer constant CTA

$$Z = C_{4H_9} - S^* C_{tr,RAFT} > 10$$
; high transfer constant CTA

(B)  $\frac{100}{0.5} = 0.00$ 

$$\frac{1.1}{0.5} = 0.00$$

$$\frac{1.1}{0.05} = 0.00$$
(C)  $\frac{1.1}{0.05} = 0.00$ 
(D)  $\frac{100}{0.05} = 0.00$ 
(D)  $\frac{100}{0.05} = 0.00$ 
(D)  $\frac{100}{0.05} = 0.00$ 
(E)  $\frac{1.1}{0.05} = 0.00$ 
(D)  $\frac{100}{0.05} = 0.00$ 
(D)  $\frac{100}{0.05}$ 

Figure 1. (A) RAFT scheme for the polymerization of styrene (S). Kinetic simulations as a function of the chain transfer constant (C<sub>tr.RAFT</sub>) from 1 to 500: (B) change in DP vs conv., (C) change in dispersity vs conv., (D) change in conversion vs time. Construction of square distribution using 3 MWDs with D = 2: (E)  $M_p s = 2.5 k$  (0.42), 8k (0.21), and 20k (0.37). (F)  $M_p s = 20k$  (0.46), 50k (0.08), and 120k (0.46). (G) Comparison of (E) and (F). The log-weight distribution (x(M)) was used to construct the square distributions.

techniques, however, are not amenable to precise control over both shape and breadth of the MWD in a one-pot, batch reaction.

For reversible-addition fragmentation chain transfer (RAFT)-mediated polymerizations in which the RAFT agent transfer dominates over conventional free-radical transfer and termination, the degree of polymerization (DP) and dispersity (D) can be ultimately tuned (see Figure 1B,C). 11,12 The higher transfer constant  $(C_{tr.RAFT} > 10)$  results in a linear increase in DP with conversion and a narrow MWD (i.e.,  $\mathcal{D}$  <1.1), while a C<sub>tr,RAFT</sub> of ~1 produces polymers with a DP independent of conversion and a broader MWD (D = 2). Regardless of the transfer constant and resulting dispersity, all polymer chains have RAFT end groups, which can further be used in chain extension polymerizations. It has been demonstrated that by tuning the transfer constant of a single RAFT agent, the dispersity could readily be tuned, providing an additional level

of control over the MWD<sup>13,14</sup> with  $\mathcal{D}$  ranging between 1 and 2, and now using mixed RAFT agents has produced the same outcome. 15,16

Polymer blending is the simplest method to control the shape of the MWD to gain desired polymer properties and is routinely used in the industry. The rheological consequences of a given MWD have been quantified and exploited in the direction of achieving a desired material response.<sup>17</sup> However, not being able to reproducibly and consistently produce the starting polymers with the same MWD prior to mixing has been a major challenge. Recent attempts to overcome this blending hurdle are to create the desired overall MWD directly through the polymer synthesis by modifying the polymerization kinetics through machine learning-assisted kinetic modeling, <sup>18</sup> controlling catalytic reactivity, <sup>13–15</sup> and flow chemistry. <sup>19,20</sup> These recent methods rely on predictive and, in most cases, complex modeling of the polymerization.<sup>2</sup>

Log M

Here, we demonstrate that synthesis of the starting polymers through RAFT control provides a simple, reproducible, scalable, and, importantly, almost kinetic model-free method. By using only a mixture of a few of these starting polymers, we are able to produce near-square, slanted, and even chair-shaped MWDs, with high predictability. The key concept relies on the basic understanding of the RAFT mechanism, 11 allowing the reproducible synthesis of well-defined starting polymers with Gaussian distributions<sup>22</sup> and a dispersity index close to 2 by using a RAFT agent with a  $C_{tr,RAFT}$  close to 1 (see Figure 1C). The method of blending polymers with D close to 2 described here has generality to all polymers regardless of the polymerization technique and regardless of the types of polymers being mixed. The consequences of MWD on the macroscopic properties of polymers can be significant. Of prime importance are the rheological properties. Given that commercial polymers are typically polydisperse, an enormous effort was put into understanding the role of dispersity on the viscoelastic and processing response. <sup>17</sup> In this context, the socalled inverse problem, i.e., extracting the MWD from the measured rheology, has been an outstanding rheological challenge with crucial implications in processing.

#### EXPERIMENTAL SECTION

**Materials.** The following reagents were used as received: activated basic alumina (Aldrich: Brockmann I, standard grade, ~150 mesh, 58 Å), silica gel 60 (230–400 mesh ATM (SDS)), ethyl 2-bromopropionate (Sigma Aldrich Co., 99%), potassium ethyl xanthogenate (Sigma Aldrich Co., 99%), TLC plates (silica gel 60 F254). 2,2'-Azobis(2-methylpropionitrile) (AIBN) (98%, Fluka) was purified by recrystallization from methanol before use.

The following solvents were used as received: ethanol (Chem-Supply, AR grade), acetone (Chem-Supply, AR grade), dichloromethane (DCM: Chem-Supply, AR grade), ethyl acetate (EtOAc: Chem-Supply, AR grade), petroleum spirit 40−60 °C (Thermo Fisher Scientific, AR grade), methanol (MeOH: Merck, 99.9%, HPLC grade), tetrahydrofuran (THF: Merck, 99.9%, HPLC grade), toluene (Merck, 99.9%, HPLC grade), and chloroform-d (Sigma Aldrich Co., ≥99.8 atom % D, contains 0.5 wt % silver foil as a stabilizer).

Styrene (Sigma Aldrich Co., >99%) was passed through a basic alumina column to remove an inhibitor and then used in the polymerizations.

Nuclear Magnetic Resonance (NMR). All <sup>1</sup>H NMR spectra were recorded on a Bruker DRX 400 MHz spectrometer at 25 °C using an external lock (CDCl<sub>3</sub>) and referenced to the residual non-deuterated solvent (CHCl<sub>3</sub>).

Size-Exclusion Chromatography (SEC) Calibrated with Linear Polystyrene (PS). All polymer samples were dried prior to analysis in a vacuum oven for 24 h at 50 °C. The dried polymer was dissolved in tetrahydrofuran (THF) to a concentration of ~20 mg/mL and then filtered through a 0.45  $\mu m$  PTFE syringe filter. Analysis of the molecular weight distributions of the polymers was accomplished using a Waters 2695 separations module, fitted with a Waters 410 refractive index detector maintained at 35 °C, a Waters 996 photodiode array detector, and two Ultrastyragel linear columns (7.8 mm × 300 mm) arranged in series. These columns were maintained at 40 °C for all analyses and are capable of separating polymers in the molecular weight range of  $(500-4) \times 10^6$  g/mol with high resolution. All samples were eluted at a flow rate of 1.0 mL/min. Calibration was performed using narrow molecular weight PS standards ( $\theta \le 1.1$ ) ranging from 500 to 2 million g/mol. Data acquisition was performed using Empower software, and molecular weights were calculated relative to polystyrene standards.

Synthesis of Ethyl 2-((Ethoxycarbonothioyl)thio)propanoate (MADIX Agent: Macromolecular Design by Interchange of Xanthates). Ethyl 2-bromopropionate (5.00 g, 27.6 mmol) was dissolved in 100 mL of ethanol, and the solution was cooled down in

an ice bath. Potassium ethyl xanthogenate (4.90 g, 30.38mmol) was then slowly added over a period of 30 min. The solution was light yellow and turbid, and the reaction mixture was stirred at room temperature for 24 h. It was noted that after ~10 h during the reaction, the solution turned white. The reaction mixture was then filtered (to remove KBr), and the solvent was removed by rotoevaporation. The crude product was purified by column chromatography using silica gel (petroleum spirit/ethyl acetate (v/v) = 10/1,  $R_f = 0.61$ ). A light-yellow liquid product was obtained to give a yield of 79% (4.865 g). <sup>1</sup>H NMR (400 MHz, CDCl<sub>3</sub>):  $\delta = 4.60-4.65$  (q, J = 7.12 Hz, 2H), 4.34-4.39 (q, J = 7.4 Hz, 1H),4.17-4.22 (q, J = 7.12 Hz, 2H), 1.55-1.56 (d, J = 7.4 Hz, 3H), 1.39-1.42 (t, J = 7.12 Hz, 3H), and 1.25-1.29 (t, J = 7.12 Hz, 3H).

Solution Polymerization of Styrene with MADIX in Toluene. General procedure: The monomer (styrene), MADIX agent (molar ratios [styrene]/[MADIX]= 25, 80, 100, 200, 400, and 800), and AIBN (molar ratios [MADIX]/[AIBN] = 10) were weighed into a 50 mL Schlenk tube, and the mixture purged with Ar(g) for 30 min. Toluene was purged separately in another vial for 30 min. Toluene (at a volume fraction of 40%) was transferred to a Schlenk tube to dissolve the reactant, and then purged for another 10 min with Ar(g). The polymerization was started at 70 °C under Ar(g) and allowed to polymerize for 15 h. The polymerization was quenched with liquid N<sub>2</sub> and exposed to air. A droplet of the solution was dissolved in CDCl<sub>3</sub> to check the conversion by <sup>1</sup>H NMR. The polymer solution was diluted with DCM and then precipitated in 300 mL of methanol to remove impurities and unreacted monomers. After precipitation, the solvent was removed by vacuum filtration, and the polymer was collected as white powder and dried in a high vacuum oven at 50 °C overnight.

Six different PSTY samples were synthesized in triplicate according to the procedure discussed above (see Table S1 in the Supporting Information). The six polymers used to construct the various shaped MWDs are given in Table 1.

Table 1. Polystyrene Used to Construct the Different Shaped  $MWDs^a$ 

polymer	conversion	$M_{\rm n}({ m g/mol})$	$M_{\rm p}({\rm g/mol})$	Đ
A	0.55	3050	5390	1.92
В	0.40	9470	17 700	1.86
C	0.35	11 170	22 300	1.88
D	0.29	19 010	34 160	1.87
E	0.24	38 290	67 630	1.84
F	0.17	60 000	109 630	1.85

<sup>a</sup>The average-number molecular weight  $(M_n)$  and the peak molecular weight  $(M_p)$  from the log-weight distribution (x(M)). The polymers were precipitated to remove impurities, and this process may further remove low molecular weight oligomers resulting in a slight decrease in D.

Blending of Polystyrene Polymers. All blends were carried out in an identical procedure. For SB1, for example (see Figure 5 below), we added 28.1 mg of S6 and 71.7 mg of S9 into a vial. The two polymers were dissolved in 5 mL of THF and shaken for 3 h at ambient temperature to produce a homogeneously mixed sample. The solution was then concentrated to  $\sim$ 1 mL. We then added 10 mL of methanol to precipitate the polymer. The solvents were then removed by first a nitrogen gas flow and then dried fully under high vacuum for 24 h to produce a white solid. This sample was analyzed by SEC to determine its MWD and then used for rheological testing.

Rheometry. To perform rheological measurements, the samples were first shaped in a disc form with the help of a homemade mold connected to a hydraulic press and then annealed overnight at 150 °C in a vacuum oven. This treatment did not cause degradation as confirmed by the reproducibility of measurements and self-consistency of extracted data. Afterward, the samples were reshaped to 8 or 4 mm discs using the hydraulic press under vacuum and were

heated to  $T_{\rm g}$  + 50 °C for 30 min. Subsequently, the samples were pressed using either the hydraulic or manual press to reach their final shape. This procedure was necessary to ensure that the samples were macroscopically homogeneous without any evidence of air bubbles.

Rheological measurements were performed with a strain-controlled ARES rheometer (TA Instruments) equipped with a force rebalance transducer 2KFRTN1 and a convection oven, ensuring accurate temperature control (±0.1 °C). For the experiments, a stainless-steel plate-plate geometry with diameters of 8 and 4 mm diameter was used. The 4 mm geometry was necessary for low-temperature measurements near the glass transition, where the sample became stiff. The samples were loaded on the rheometer and allowed to melt and homogenize at temperatures ranging from 140 to 160  $^{\circ}\text{C}$  for about 60 min. In addition, a MCR 702 rheometer (Anton Paar, Austria), equipped with a CTD-180 hybrid oven, which provides a temperature control (±0.1 °C) by means of a Peltier and convection system, was also used. The same procedure as with the ARES rheometer was followed. All experiments were performed in the presence of nitrogen to provide an inert atmosphere. Measurements were performed at both strain-controlled and stress-controlled modes to probe the material response to oscillatory and steady stress (creep), respectively.

Dynamic strain amplitude sweep tests were performed at a constant angular frequency and temperature and varying strain amplitude to determine the (strain amplitude) range of linear viscoelastic (LVE) response, where the values of the storage and loss moduli,  $G'(\omega)$  and  $G''(\omega)$ , respectively, do not depend on the strain. The dynamic frequency sweep test provided information on the frequency spectrum of the investigated material, where a strain signal with constant amplitude and varying frequency (from 10<sup>2</sup> to 10<sup>-2</sup> rad/s) was imposed, and the stress response was recorded, revealing  $G'(\omega)$  and  $G''(\omega)$ . The samples were measured over a wide range of temperatures, and by using the principle of Time-Temperature Superposition (TTS), it was possible to construct linear viscoelastic master curves for each specific sample. The LVE data at each temperature were shifted with respect to a selected reference temperature  $(T_{ref})$  by a horizontal shift factor  $(a_T)$  and a vertical shift factor  $(b_T)$ . The horizontal (frequency) shifting was performed manually by shifting the data until they collapsed with each other. The respective shift factor is described by the WLF equation

$$\log a_T = -\frac{c_1(T - T_{\text{ref}})}{c_2 + (T - T_{\text{ref}})} \tag{1}$$

where  $c_1$  (unitless) and  $c_2$  (in K) are fit parameters.

The vertical (modulus) factor,  $b_T$ , is given from the equation

$$b_T = \frac{\rho_{\text{ref}} T_{\text{ref}}}{\rho \times T} \tag{2}$$

where  $\rho$  is the temperature-dependent density and for polystyrene is given by this equation  $^{26}$ 

$$\rho(T) = (1.2503 - 6.05) \times 10^{-4} T \text{ [K] in g/cm}^3$$
(3)

Measurements at high frequencies near the glass transition were affected by instrument compliance, and appropriate action was taken to account for it and correct them accordingly.<sup>27</sup>

Linear viscoelastic spectra were also used to determine the rheological glass transition temperature  $(T_{\rm g})$  of the measured samples (see table in Figure 5 later in the text). The values of the WLF coefficients at 150 °C were  $C_1=7.2$  and  $C_2=103$ K, identical with those of reference.<sup>28</sup>

*Data Analysis Based on Viscoelastic Modeling.* For unentangled polymers of molar mass *M*, the memory function of the Rouse model is

$$f_{\text{Rouse}}(t, M) = \sum_{p=1}^{\infty} \exp\left(\frac{-p^2 t}{\tau_{\text{R}}(M)}\right)$$
(4)

By using the approach adopted by van Ruymbeke, <sup>29</sup> the Rouse time can be expressed as

$$\tau_{\text{Rouse}}(M) = KM^2 \tag{5}$$

where K is a material coefficient which scales as  $\frac{\tau_e(T)}{M_e^2}$ ,  $M_e$  is the Kuhn molar mass of an entanglement segment, and  $\tau_e$  is the relaxation time of an entanglement strand. As  $\tau_e$  depends on the temperature, K is a temperature-dependent coefficient. The stress relaxation modulus G(t, M) is expressed as

$$G(t, M) = \sum_{M_{\min}}^{M_{\max}} \frac{\rho RT}{M} f_{\text{Rouse}}(t, M) w(M)$$
(6)

To obtain the best fit of the observed data, K takes the value of  $\sim$ 4  $\times$   $10^{-10}$  s  $(\text{mol/g})^2$  at  $T_{\rm g}$  + 30 °C, which is considered to be reasonable. In fact, based on the scaling of K above, its ratio at two temperatures should be very close to the respective ratio of  $\tau_{\rm e}$ ,  $^{29,30}$  which is actually confirmed here. Indeed, van Ruymbeke  $^{29}$  reported K = 2  $\times$   $10^{-12}$  s  $(\text{mol/g})^2$  for entangled polystyrenes at T = 170°, corresponding to a  $\tau_{\rm e}$  = 0.00013. In our case,  $\tau_{\rm e}(T_{\rm g}$  + 30 °C) = 0.025 s and K = 4  $\times$   $10^{-10}$  s  $(\text{mol/g})^2$ . That is, the ratio of K equals the ratio of  $\tau_{\rm e}$ .

The relaxation dynamics of entangled polymers are described as the sum of three relaxation modes, fast Rouse, longitudinal, and reptation. The fast Rouse relaxation modes can be expressed by the equation below, where  $M/M_{\rm e}$  is the number of entanglement strands per chain.

$$f_{\text{F,Rouse}}(t, T, M) = \frac{M_{\text{e}}}{M} \sum_{p=M/M_{\text{e}}}^{M} \exp\left(-\frac{2p^2t}{\tau_R(T, M)}\right)$$
 (7)

Here, we consider  $\tau_{\rm R}(M)=\tau_{\rm e}M^2/M_{\rm e}^2$ , with  $\tau_{\rm e}$  being the experimental value and  $M_{\rm e}$  equal to 17.5 kg/mol.

The longitudinal mode function (along the confining tube) can be described by Rouse modes. It originates from the fact that because different tube segments before deformation are oriented differently, they also stretch differently, and hence, redistribution of monomers along the tube takes place after the deformation. It was shown<sup>31</sup> that these relaxation modes contribute to the relaxation of 1/5 of the total stress stored in the tube

$$f_{\text{Long}}(t, M) = \frac{M_e}{5M} \sum_{p=1}^{M/M_e-1} \exp\left(-\frac{2p^2t}{\tau_R(M)}\right)$$
 (8)

Both fast Rouse and longitudinal modes are active for relaxation times up to the Rouse time of the chain, and hence, we consider them as components of the effective Rouse contribution. Note that the glassy dynamics at high frequencies is not considered in the present work.

For polydisperse entangled polymers, the effective Rouse contribution to the stress relaxation modulus  $G_{\text{Rouse}}(t, M)$  becomes

$$G_{\text{Rouse}}(t, M) = \sum_{M_{\text{min}}}^{M_{\text{max}}} \frac{\rho RT}{M_e} [f_{\text{F,Rouse}}(t, M) + f_{\text{Long}}(t, M)] w(M)$$
(9)

where  $\rho$  is the polymer density, R is the universal gas constant, and  $w(M) = dW(M)/d\log(M)$  with the weight fraction of all chains having a molar mass below M.

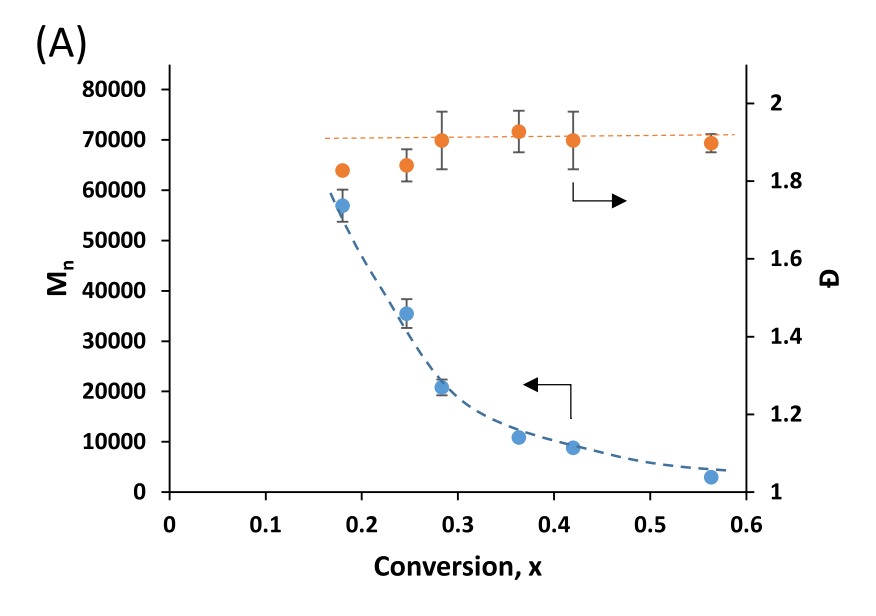
Along the same lines, a simplified way to describe the entanglement relaxation function by accounting for dynamic tube dilution (DTD) is provided by des Cloizeaux $^{32}$ 

$$F_{\text{DTD}}(t, M) = \frac{\pi}{8} \sum_{p \text{ odd}} \frac{1}{p^2} \exp(-p^2 U(t))$$
 (10)

The function U(t) is

$$U(t, M) = \frac{t}{\tau_{\text{rep}}} + \frac{M_{\text{e}}}{M} g \left[ \frac{tM}{\tau_{\text{rep}} M_{\text{e}}} \right]$$
(11)

with



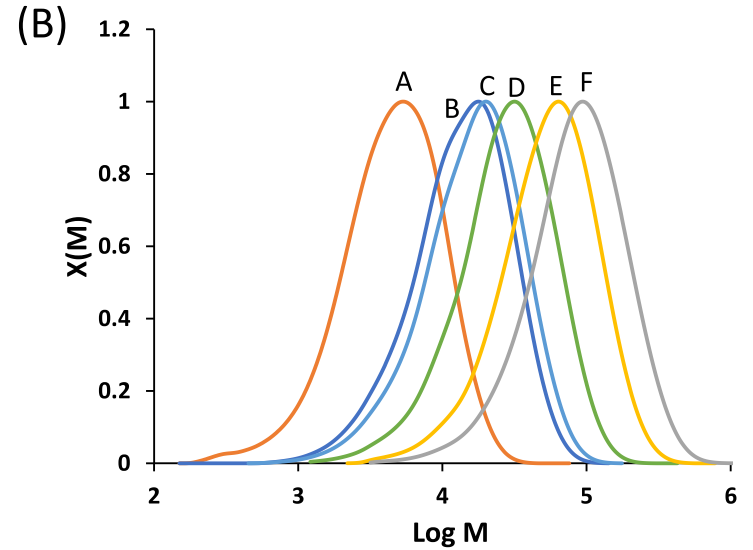


Figure 2. (A) Solution polymerizations of styrene with an MADIX agent at 70  $^{\circ}$ C using three replicate polymerizations.  $M_{\rm n}$  and D vs conversion (see Table 1). (B) Molecular weight distributions (MWDs) of polymers A–F in Table 1 as determined by SEC.

$$g(y) = \sum_{n=1}^{\infty} \frac{1 - \exp(-n^2 y)}{n^2}$$
 (12)

The first term of the equation for U(t, M) represents the relaxation by reptation, whereas the second term represents the contribution of contour length fluctuations. The terminal relaxation time, which we typically call reptation time (even if it encompasses non-reptative mechanisms as mentioned above), is defined as

$$\tau_{\rm rep}(M) = \tau_{\rm e} \left(\frac{M}{M_{\rm e}}\right)^{3.4} \tag{13}$$

The reptation contribution to the total stress relaxation modulus can be expressed as follows

$$G_{\text{rep}}(t, M) = \frac{\rho RT}{M_{\text{e}}} \sum_{M_{\star}}^{\infty} [F_{\text{DTD}}(t, M)]^{\beta} w(M)$$
 (14)

where the exponent  $\beta$  is set to a value of 2, according to the double reptation concept.<sup>33</sup> It is now possible to evaluate the total stress relaxation modulus by summing the above equations for effective Rouse and reptation contributions

$$G(t, M) = G_{\text{Rouse}}(t, M) + G_{\text{rep}}(t, M)$$
(15)

For samples that are at the transition between entangled and unentangled regime, the total stress relaxation modulus was calculated as the sum of two contributions, unentangled and entangled, each weighted by the fraction of short and long chains, respectively, based on the SEC characterization of table in Figure 5

$$G(t, M) = \phi_{\text{unentangled}} G_{\text{unentangled}}(t, M) + (1 - \phi_{\text{unentangled}})$$

$$G_{\text{entangled}}(t, M)$$
(16)

### RESULTS AND DISCUSSION

The average degree of polymerization (DP) and dispersity index ( $\mathcal{D}$ ) for a RAFT-mediated polymerization is controlled by the  $C_{\rm tr,RAFT}$ . At a  $C_{\rm tr,RAFT}$  of 1, both the DP and  $\mathcal{D}$  reached a maximum and constant value independent of conversion (curve a in Figure 1B,C). Increasing  $C_{\rm tr,RAFT}$  to values greater than 1 showed that the DP and  $\mathcal{D}$  profiles were conversion dependent, which became pronounced at higher  $C_{\rm tr,RAFT}$  values. Theoretically, the rate of polymerization will not be

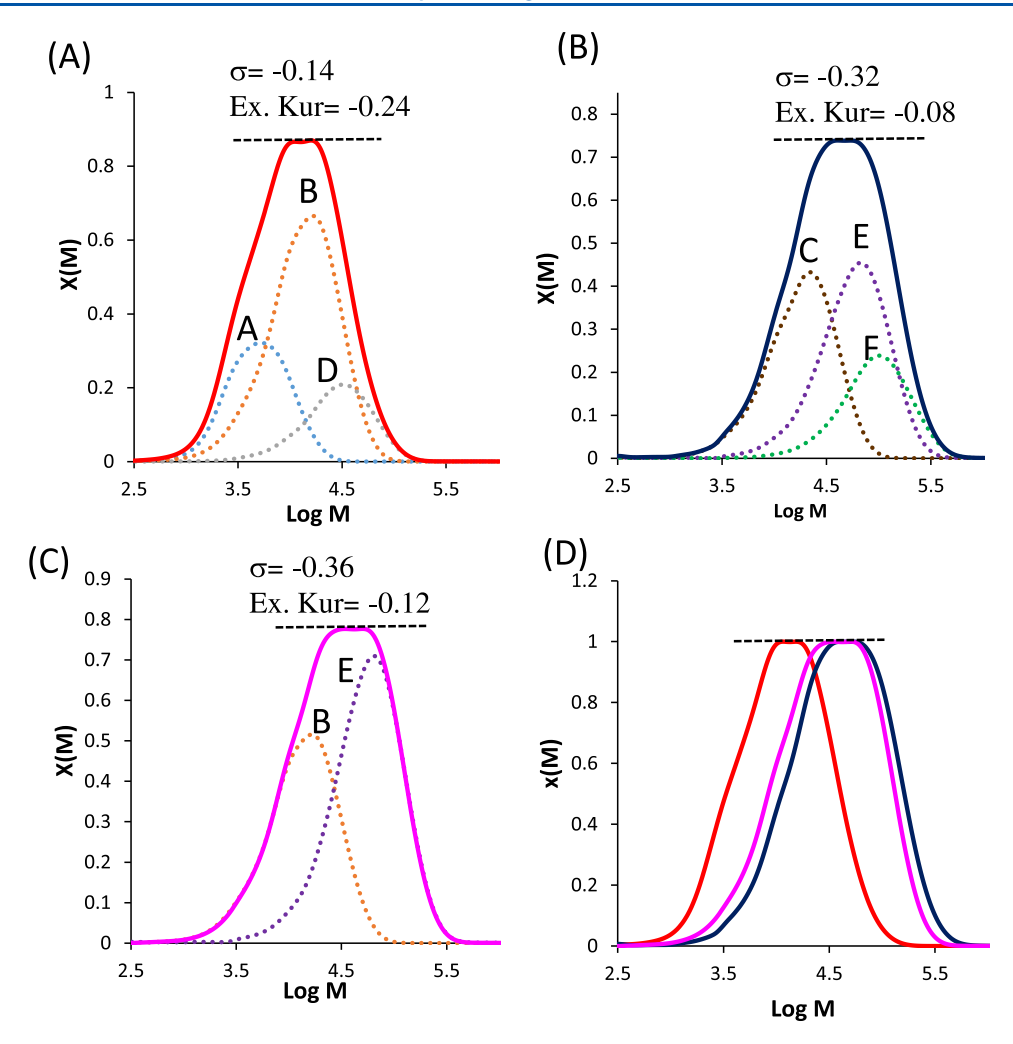


Figure 3. Experimental square-shaped MWDs constructed from the polymers A–F in Table 1. (A) Square#1 constructed from A (28 wt %), B (55 wt %), and D (17 wt %); (B) Square#2 constructed from C (42 wt %), E (39 wt %), and F (19 wt %); (C) Square#3 constructed from B (43 wt %) and E (57 wt %); and (D) comparison of the three square distributions. MWD data for these were given in Table S2 in SI.

influenced by the presence of the RAFT agent, and conventional free-radical kinetics including the appropriate chain-length dependent termination<sup>34</sup> can be used to model the system. 11,35 In general, to maintain a RAFT-dominated mechanism, the RAFT to initiator concentration should be kept at ratios greater than 10:1. Simulations of the rate of polymerization for styrene (Figure 1A,D) showed that when targeting higher DPs, the lower initiator concentration resulted in a lower polymerization rate, making it difficult to make the same polymer with the same MWD from batch to batch. The only exception was the use of a RAFT agent with a Ctr.RAFT equal to or close to 1. Here lies the key concept of our work. In the case of the polymerization of styrene, acrylamide, and other monomers in the presence of a MADIX agent (where  $C_{\rm tr,RAFT} \sim 1$ , Figure 1A),  $^{36-42}$  the constant DP and  $\mathcal D$  profiles suggest that these types of polymerizations will produce the same MWD regardless of conversion, providing a mechanistically facile, kinetic model-free, and reproducible route to generating polymers with identical MWDs. This process will have industrial appeal for the reproducible production at the scale of unusual and predictable MWDs by blending polymers of different DPs with a  $D \sim 2$  (see below).

Simulation of mixing polymers of different DPs to produce a square MWD is shown in Figure 1E-G. Gaussian distribu-

tions<sup>22,43</sup> were generated for each DP at D=2, and a mixture of three MWDs gave the resulting square distribution. For example, mixing three MWDs with peak molecular weights  $(M_p s)$  at 2500, 8000, and 20 000 g/mol produced a square MWD (i.e., "differential log molecular weight,"  $x(M)^{44}$ ) at 42, 21, and 37 wt %, respectively (Figure 1E). The square MWD can be shifted to a higher molecular weight by increasing the  $M_p s$  to 20 000, 50 000, and 120 000 g/mol at 46, 8, and 46 wt %, respectively (Figure 1F), which is more clearly illustrated in Figure 1G. These simulations demonstrate that only three polymers are required to generate a square MWDs and that control of a desired square MWD can be generated using this blending method.

We carried out RAFT-mediated polymerizations of styrene using a MADIX agent ( $C_{\rm tr,RAFT} \sim 1$ ), using three replicate polymerizations for each targeted DP (see Table S1 in S1). The reproducibility of the resulting number-average molecular weight ( $M_{\rm n}$ ) was excellent (Figure 2A). Decreasing the targeted  $M_{\rm n}$  resulted in higher conversions due to the higher initiator concentration. We found that regardless of conversion or  $M_{\rm n}$ , the dispersity index for all polymerizations was close to 1.9 after polymer purification by precipitation. This agrees with our hypothesis that the low RAFT transfer constant could produce the same  $M_{\rm n}$  and D regardless of conversion. The

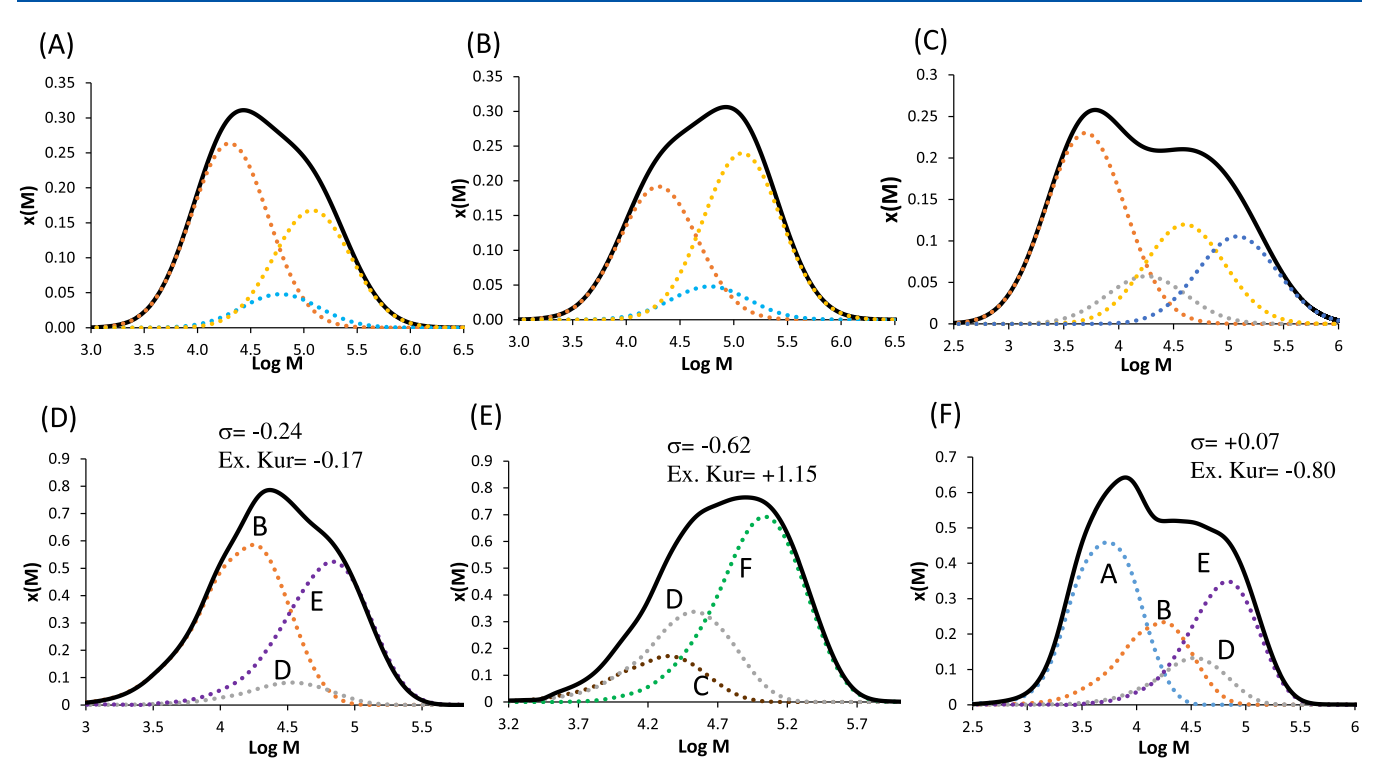


Figure 4. Simulated distributions using log-normal distribution method by blending polymers with different peak molecular weights  $(M_ps)$  and all with dispersity = 2: (A)  $M_ps$  = 10k (55 wt %), 30k (10 wt %), and 60k (35 wt %); (B)  $M_ps$  = 10k (40 wt %), 30k (10 wt %), and 60k (50 wt %); (C)  $M_ps$  = 2.5k (45 wt %), 8k (11 wt %), 20k (23 wt %), and 60k (21 wt %). Experimental MWDs constructed from the polymers A–F in Table 1: (D) Slanted#1: B (28 wt %), D (55 wt %), and E (17 wt %); (E) Slanted#2: C (14 wt %), D (31 wt %), and F (55 wt %); and (F) Chair: A (40 wt %), B (20 wt %), D (12 wt %), and E (28 wt %).

individual polymers used to construct the square and other MWD shapes were all monomodal and Gaussian (Figure 2B, and the MWD data given in Table 1).

A measure of the symmetry of a normalized distribution about the mean<sup>45</sup> can be determined using the skewness factor,  $\sigma$ , based on the third moment (eq 17), and the excess kurtosis, Ex. Kur., a measure of the peak shape, given by the fourth moment in eq 18 (where  $x_i$  is the  $\log M$  at  $M_i$ ,  $y_i$  is the frequency,  $\overline{x}$  is the mean, and S is the standard deviation of the distribution)

$$\sigma = \frac{\sum_{i=1}^{n} \gamma_i (x_i - \overline{x})^3}{S^3} \tag{17}$$

Ex. Kur. = 
$$\frac{\sum_{i=1}^{n} y_i (x_i - \overline{x})^4}{S^4} - 3$$
 (18)

To construct the square-shaped or other MWDs, we first used the simulations above as a guide on the choice of polymer mixtures and their respective weight fractions to obtain the desired overall MWD for the differential log molecular weight distribution (x(M)). A mixture of three polymers A, B, and D (from Table 1 and Figure 2B) at 28, 55, and 17 wt %, respectively, allowed the experimental blending construction of a near-square MWD (Figure 3A). It can be seen that a substantial portion of the x(M) distribution has a near constant (i.e., near flat) profile with an excess kurtosis of -0.24 interpreted as platykurtic. There is also a slight broadening toward the low molecular weight part of the distribution, suggesting a slightly negative skewed distribution ( $\sigma = -0.14$ ). An experimental square MWD with a higher molecular weight can be constructed by mixing polymers C, E, and F at 42, 39,

and 19 wt %, respectively (Figure 3B). In this case, the flat portion of the distribution extends to a larger molecular weight range, with an excess kurtosis of -0.08 and a slightly negatively skewed distribution ( $\sigma = -0.32$ ). We could even construct a square MWD by mixing two polymers, B and E, at 43 and 57 wt %, respectively (Figure 3C). Here, the MWD profile is similar to the mixture of C, E, and F (Figure 3B) and has similar skewness and kurtosis values to the other two square-like distributions. The MWD average data for these three square-shaped MWDs were given in Table S2 in SI. The three square-shaped MWDs shown in Figure 3D demonstrate the fine control over the MWD and relative ease in constructing these unusual MWDs without invoking complex kinetic modeling.

Simulations using Gaussian distributions (i.e., generated for each DP at  $\theta = 2$  could be used to control the shape of the distributions with a positive or negative slant and a chair conformation (Figure 4A-C). For the negative and positive slanted distributions, the mixture of the same three polymers  $(M_n$ s equal 10k, 30k, and 60k) was used but in different ratios. The positive distribution was constructed at 55, 10, and 35 wt % (Figure 4A), while the negative distribution was constructed at 40, 10, and 50 wt % (Figure 4B). In constructing the chair conformation, a mixture of four polymers with  $M_n$ s equals 2.5k, 8k, 20k, and 60k at 45, 11, 23, and 21 wt %, respectively (Figure 4C). Experimentally, the positive distribution was constructed using polymers B, D, and E from Table 1 at 51, 7, and 42 wt %, respectively (Figure 4D). The shape was similar to the simulation, with a slight negative skewness ( $\sigma = -0.24$ ) due to the long low molecular weight tail. The positive slanted distribution was also demonstrated using a mixture of polymers

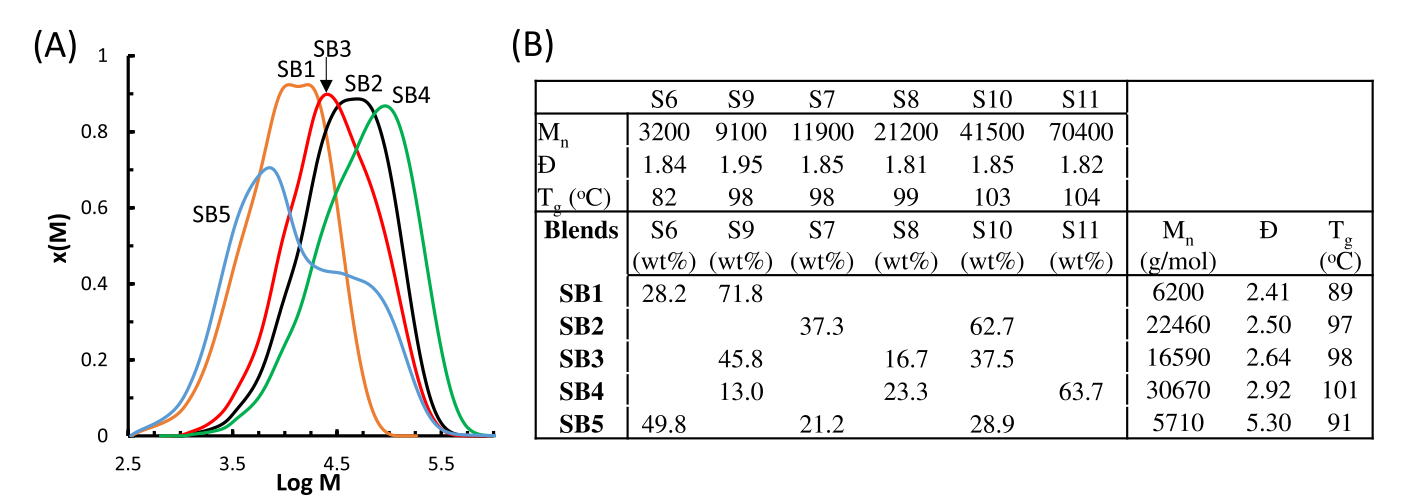


Figure 5. (A) Experimental log-weight distributions (x(M)) for the blends (SB) made by blending polymers (S) at different weight ratios. (B) MWD data for the starting polymers and blends and glass transition temperatures  $(T_g)$  for all polymers and blends.

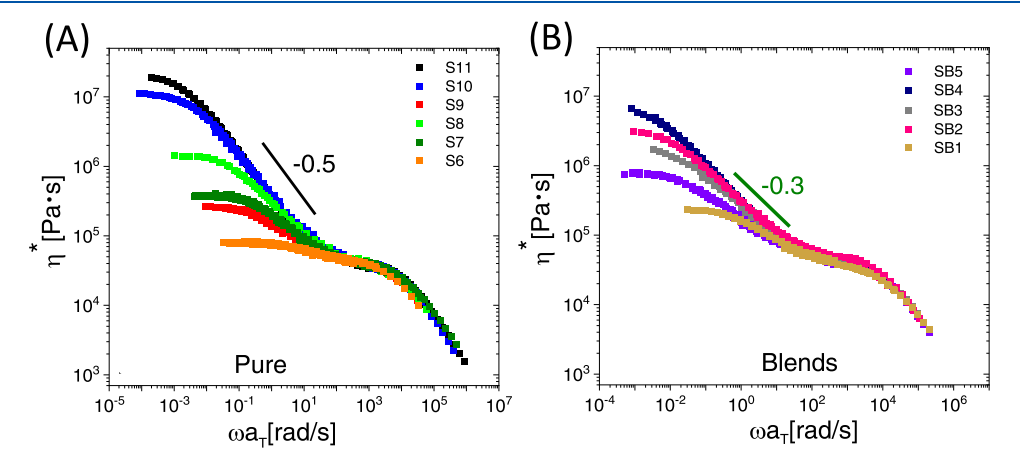
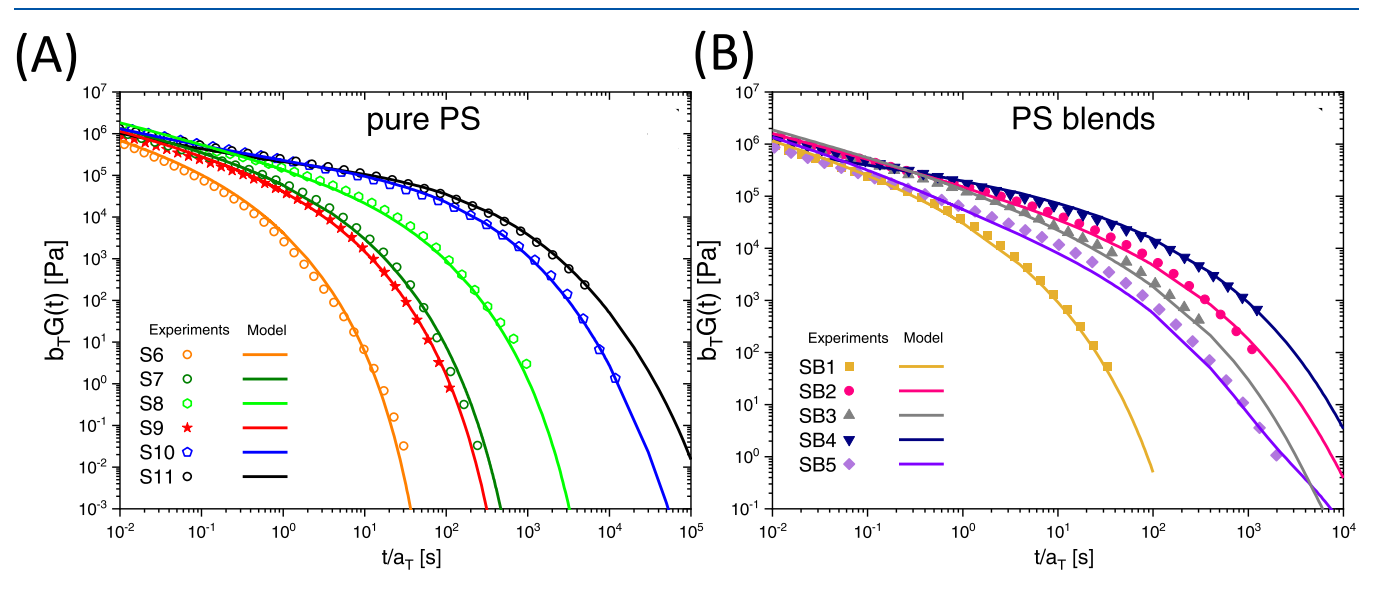


Figure 6. Complex viscosity as a function of shifted oscillatory frequency at  $T_{\text{ref}} = T_{\text{g}} + 30$  °C for pure polystyrene samples (A) and their blends (B). Lines with slopes of -0.5 and -0.3 are also shown, reflecting Rouse and Zimm scaling, respectively (see text).



**Figure 7.** Shifted stress relaxation modulus as a function of shifted time (exacted by Fourier transformation of the frequency-dependent G' and G'' data of Figure S1). Symbols and lines represent data and model predictions, respectively. Graph A refers to the pure polystyrene, whereas graph B refers to the blends. The temperature was  $T_{\text{ref}} = T_{\text{g}} + 30$  °C.

C, D, and F at 14, 31, and 55 wt %, respectively (Figure 4E); but in this case, the skewness was moderately negative ( $\sigma$  =

-0.62). Using a mixture of A, B, D, and E at 40, 20, 12, and 28 wt % produced the chair distribution (Figure 4F) with a

slightly positive skewness ( $\sigma$  = +0.07). The MWD average data for these unusually shaped MWDs were given in Table S2 in S1

**Linear Viscoelasticity.** The samples investigated by rheometry are reported in Figure 5 together with their molecular weight characteristics and glass transition temperature  $(T_{\sigma})$ .

Figure 6 depicts the complex viscosity master curves extracted from the moduli of Figure S1 in the SI for the pure polystyrenes and their blends (see table in Figure 5) at the same distance from  $T_{\rm g}$  ( $T_{\rm ref}=T_{\rm g}+30~{\rm °C}$ ). At high frequencies, the curves overlap because of the same segmental behavior (consistent with Figure S1A,C in the SI). At the other end of the spectrum, a low-frequency Newtonian plateau regime is detected, followed by thinning. The latter regime develops more clearly for the larger molar masses (samples S10, S11) and is characterized by a scaling  $\eta^* \sim \omega^{-1/2}$  that conforms to the Rouse prediction of monodisperse linear polymers. On the other hand, the power-law exponent for lower molar mass polymers ranges from -0.32 to -0.37. This scaling is consistent with the Zimm model,  $\eta^* \sim \omega^{-1/3}$ , and may reflect the dilution effect of the smaller molar mass tails, which act as effective solvents.

The LVE master curves of Figure S1 in the SI can be Fourier-transformed into stress relaxation modulus G(t) data, which are depicted in Figure 7 for both pure polystyrene samples (graph A) and blends (graph B). By accounting for the exact molar mass distribution, as determined in Figure 5, we use the appropriate model presented above and accurately describe the G(t) for all tested samples, as shown in Figure 7. Samples S11, S10, and SB4 are (marginally to weakly) entangled, whereas the rest of the samples are unentangled. We used  $\tau_{\rm R}(M) = \tau_{\rm e} M^2/M_{\rm e}^2$ , with  $\tau_{\rm e}$  being the experimental value of 0.042s at  $T_{\rm g}$  + 30 °C,  $M_{\rm e}$  = 17.5 kg/mol, and the double reptation exponent  $\beta = 2$ . For the unentangled polymers, we used one fit parameter,  $K = 5 \times 10^{-10}$  s (mol/ g)<sup>2</sup>. The satisfactory modeling of the G(t) data suggests that it is possible to use the outlined methodology to describe, or even predict, the dynamics with blends with complex MWD of any shape. Note that for SB5, the model seems to predict a high-M mode (Figure 7B), which is due to the tail of the MWD. To assess its influence on the rheology of the blend, we performed creep measurements. The time evolution of the creep compliance J(t) was measured at 130 °C and converted into frequency-dependent moduli G' and G'' by means of Fourier transformation, using the NLREG software. 28,47 In this way, the converted moduli extend the LVE master curve and the complete frequency spectrum is obtained (Figure 8). The excellent match of dynamic frequency sweep and converted creep data over a frequency range exceeding two decades and the identical J(t) for different values of the imposed steady stress confirms that the creep measurements probed the LVE response of SB5. Importantly, the extracted zero-shear complex viscosities from the initial and the complete (with creep data) frequency spectrum are virtually identical (see Figure S2). This validates the results extracted from the analysis based on Figure 7.

The zero-shear viscosity  $(\eta_0)$  values for the pure polymers and their blends were determined from the complex viscosity data of Figure 6 through standard fitting procedures (not shown) using power-law models and plotted as a function of the weight-average molar mass in Figure 9. The zero-shear

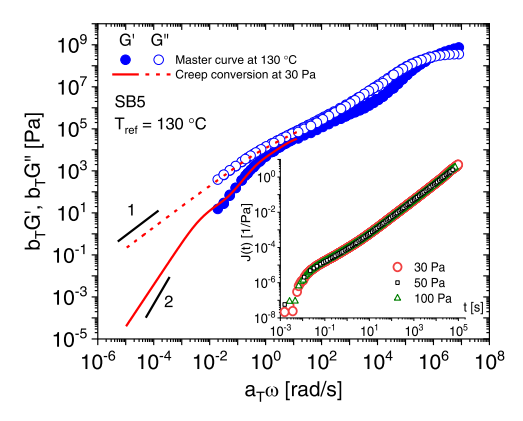
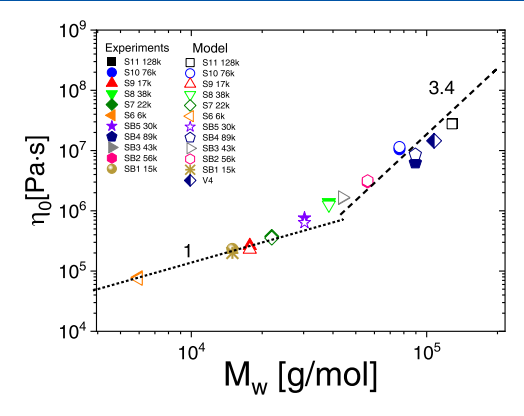


Figure 8. Complete dynamic frequency spectrum of sample SB5 at a reference temperature of 130  $^{\circ}$ C. The shifted dynamic frequency sweep data are complemented by creep compliance data (inset), which have been converted into LVE moduli by means of Fourier transformation (see text). The slow mode associated with the high molecular weight tail of Figure 5 is evident (at a shifted frequency of about 0.01 rad/s). The terminal slopes of 1 and 2 for G'' and G', respectively, are indicated.



**Figure 9.** Zero-shear viscosity as a function of weight-average molecular weight for pure polystyrenes (solid symbols) and their blends (open symbols). Half-filled lozenge represents a virtual blend (see text). Dotted and dashed lines indicate the expected power-law dependence for unentangled and entangled linear polymer chains, respectively. 46

viscosity can be also estimated from the molecular model above through the integral 46

$$\eta_0 = \int_0^t G(t) dt \tag{19}$$

and the obtained values are also reported in Figure 9 as a function of the weight-average molecular weight  $M_{\rm w}$ . In this figure, two regimes can be identified: (i) for short chains, the zero-shear viscosity follows a Rouse-type scaling  $^{46}$   $\eta_0 \sim M$  (see dotted line), (ii) whereas entangled chains comply with the  $\eta_0 \sim M^{3.4}$  power-law. We have the zero-shear viscosity values obtained from the model are within a 10% error from the experimental ones, making robust use of a molecular model for linear chains, so far only challenged with simple MWDs, to predict relaxation dynamics and viscosity.

The above point is emphasized in the following characteristic example. The SB4 blend is constituted by 13 wt % of short chains (S9—see Table in Figure 5), which slightly dilute the entangled network formed by S8 and S11. We now virtually replace 13 wt % of sample S9 with sample S11. That is, we

obtain a virtual blend constituted by 23 wt % of S8 and 77 wt % of S11. The resulting blend, called V4, has a weight-average molecular weight of 107.5k and a predicted viscosity of 1.45 ×  $10^7$  Pa s (see half-filled lozenge symbols in Figure 9). This value perfectly falls onto the expected  $\eta_0 \sim M^{3.4}$  trend, corroborating the robustness of our method. It also demonstrates the importance of shaping the MWD in the way presented above to tailor the rheology of polymers. For completeness, one should also mention that a similar result could also be obtained by using a simple mixing rule for the blend viscosity  $\eta_B^{~48}$ 

$$\eta_{\rm B}^{1/\alpha} = \sum_{i} w_i \eta_i^{1/\alpha} \tag{20}$$

where  $w_i$  is the weight fraction of component i and  $\alpha$  is the scaling exponent for viscosity with molar mass (1 for unentangled and 3.4 for entangled chains). The simplicity of this approach is of course traded off with the full relaxation dynamics obtained via the molecular model. The choice is of course dictated by the need.

## CONCLUSIONS

The key concept demonstrated in this work is that by taking advantage of a low RAFT agent reactivity, polymers can be made with molecular weight and dispersity (close to 2) being independent upon conversion. This provides a readily accessible, kinetic model-free, and reproducible synthetic methodology for polymer scale-up. It further obviates, using the blending of polymers made via this method, the requirement for system-dependent and complex kinetic modeling to produce MWDs with controlled shape, breadth, and average molecular weight. We demonstrate that by mixing between two and four polymers with different  $M_n$ s, but all with a dispersity close to 2, square-like, slanted, and chair distributions could be prepared. The concept described in this work overcomes many of the difficulties in producing unusually shaped MWDs, and this controlled blending method can be applied generally to any polymer system and for the blending of different polymer types and compositions. The consequences of tailoring viscoelastic properties are polymers through the shape of the MWD are demonstrated. Of particular importance is the potential to use the tunable shape of the MWD to achieve desired changes in the rheological properties; this is based on the relatively simple chemical procedure, coupled with rheometry and modeling. It is anticipated that such versatility in adjusting the shape of the MWD will also affect the nonlinear rheology of the blends. A further challenge would be to extend this approach to much higher molecular weights well into the entanglement regime where constraint-release effects dominate the dynamics.

#### ASSOCIATED CONTENT

# Supporting Information

The Supporting Information is available free of charge at https://pubs.acs.org/doi/10.1021/acs.macromol.2c02311.

Molecular weight distribution data for the RAFT-mediated polymerizations and the overall MWDs for the differently shaped distributions (PDF)

#### AUTHOR INFORMATION

## **Corresponding Author**

Michael J. Monteiro — Australian Institute for Bioengineering and Nanotechnology, The University of Queensland, Brisbane, QLD 4072, Australia; orcid.org/0000-0001-5624-7115; Email: m.monteiro@uq.edu.au

#### **Authors**

Yanlin Shi — Australian Institute for Bioengineering and Nanotechnology, The University of Queensland, Brisbane, QLD 4072, Australia; orcid.org/0000-0003-3596-6748

Sung-Po R. Chen — Australian Institute for Bioengineering and Nanotechnology, The University of Queensland, Brisbane, QLD 4072, Australia; ⊙ orcid.org/0000-0003-4257-3889

George Fragkiadakis – Institute of Electronic Structure and Laser, Foundation for Research and Technology Hellas (FORTH), Heraklion 70013, Greece; Department of Materials Science & Technology, University of Crete, Heraklion 70013, Greece

Daniele Parisi — Department of Chemical Engineering, Product Technology, University of Groningen, 9747 AG Groningen, The Netherlands

Virgil Percec — Roy & Diana Vagelos Laboratories, Department of Chemistry, University of Philadelphia, Philadelphia, Pennsylvania 19104-6323, United States; orcid.org/0000-0001-5926-0489

Dimitris Vlassopoulos — Institute of Electronic Structure and Laser, Foundation for Research and Technology Hellas (FORTH), Heraklion 70013, Greece; Department of Materials Science & Technology, University of Crete, Heraklion 70013, Greece; orcid.org/0000-0003-0866-1930

Complete contact information is available at: https://pubs.acs.org/10.1021/acs.macromol.2c02311

# **Funding**

The research was supported by the Australian Research Council (DP190103073) to M.J.M., and NSF-DMR-1807127 and P. Roy Vagelos Chair at Penn to V.P.

#### Notes

The authors declare no competing financial interest.

#### REFERENCES

- (1) Gentekos, D. T.; Sifri, R. J.; Fors, B. P. Controlling polymer properties through the shape of the molecular-weight distribution. *Nat. Rev. Mater.* **2019**, *4*, 761–774.
- (2) Sifri, R. J.; Padilla-Velez, O.; Coates, G. W.; Fors, B. P. Controlling the Shape of Molecular Weight Distributions in Coordination Polymerization and Its Impact on Physical Properties. *J. Am. Chem. Soc.* **2020**, *142*, 1443–1448.
- (3) Widin, J. M.; Schmitt, A. K.; Schmitt, A. L.; Im, K.; Mahanthappa, M. K. Unexpected Consequences of Block Polydispersity on the Self-Assembly of ABA Triblock Copolymers. *J. Am. Chem. Soc.* **2012**, *134*, 3834–3844.
- (4) Stürzel, M.; Mihan, S.; Mulhaupt, R. From Multisite Polymerization Catalysis to Sustainable Materials and All-Polyolefin Composites. *Chem. Rev.* **2016**, *116*, 1398–1433.
- (5) Lynd, N. A.; Meuler, A. J.; Hillmyer, M. A. Polydispersity and block copolymer self-assembly. *Prog. Polym. Sci.* **2008**, *33*, 875–893.
- (6) Odian, G.Principles of Polymerization; John Wiley & Sons, Inc.,
- (7) Matyjaszewski, K.; Davis, T. P. Handbook of Radical Polymerization; John Wiley and Sons: USA, 2002.

- (8) Percec, V.; Guliashvili, T.; Ladislaw, J. S.; Wistrand, A.; Stjerndahl, A.; Sienkowska, M. J.; Monteiro, M. J.; Sahoo, S. Ultrafast synthesis of ultrahigh molar mass polymers by metal-catalyzed living radical polymerization of acrylates, methacrylates, and vinyl chloride mediated by SET at 25 degrees C. *J. Am. Chem. Soc.* **2006**, *128*, 14156–14165.
- (9) Goto, A.; Fukuda, T. Kinetics of living radical polymerization. *Prog. Polym. Sci.* **2004**, *29*, 329–385.
- (10) Moad, G.; Rizzardo, E.; Thang, S. H. Living Radical Polymerization by the RAFT Process. *Aust. J. Chem.* **2005**, *58*, 379–410.
- (11) Monteiro, M. J. Design strategies for controlling the molecular weight and rate using reversible addition-fragmentation chain transfer mediated living radical polymerization. *J. Polym. Sci., Part A: Polym. Chem.* **2005**, 43, 3189–3204.
- (12) Monteiro, M. J. Modeling the molecular weight distribution of block copolymer formation in a reversible addition-fragmentation chain transfer mediated living radical polymerization. *J. Polym. Sci., Part A: Polym. Chem.* **2005**, *43*, 5643–5651.
- (13) Goh, Y. K.; Monteiro, M. J. Novel approach to tailoring molecular weight distribution and structure with a diffunctional RAFT agent. *Macromolecules* **2006**, *39*, 4966–4974.
- (14) Benaglia, M.; Chiefari, J.; Chong, Y. K.; Moad, G.; Rizzardo, E.; Thang, S. H. Universal (Switchable) RAFT Agents. *J. Am. Chem. Soc.* **2009**, *131*, 6914–6915.
- (15) Whitfield, R.; Parkatzidis, K.; Truong, N. P.; Junkers, T.; Anastasaki, A. Tailoring Polymer Dispersity by RAFT Polymerization: A Versatile Approach. *Chem* **2020**, *6*, 1340–1352.
- (16) Monteiro, M. J.; Sherman, S. E.; Percec, V. Precise and Accelerated Polymer Synthesis via Mixed-Ligand and Mixed-RAFT Agents. *Chem* **2020**, *6*, 1203–1204.
- (17) Dealy, J. M.; Read, D. J.; Larson, R. G. Structure and Rheology of Molten Polymers, 2nd ed.; Hanser, 2018.
- (18) Li, H. C.; Collins, C. R.; Ribelli, T. G.; Matyjaszewski, K.; Gordon, G. J.; Kowalewski, T.; Yaron, D. J. Tuning the molecular weight distribution from atom transfer radical polymerization using deep reinforcement learning. *Mol. Syst. Des. Eng.* **2018**, *3*, 496–508.
- (19) Walsh, D. J.; Schinski, D. A.; Schneider, R. A.; Guironnet, D. General route to design polymer molecular weight distributions through flow chemistry. *Nat. Commun.* **2020**, *11*, No. 3094.
- (20) Corrigan, N.; Almasri, A.; Taillades, W.; Xu, J. T.; Boyer, C. Controlling Molecular Weight Distributions through Photoinduced Flow Polymerization. *Macromolecules* **2017**, *50*, 8438–8448.
- (21) Zhang, S. S.; Qiang, J.; Liu, H. H.; Li, Y. Y. Optimization Design of Groundwater Pollution Monitoring Scheme and Inverse Identification of Pollution Source Parameters Using Bayes' Theorem. *Water Air Soil Poll.* **2020**, 231, No. 27.
- (22) Monteiro, M. J. Fitting molecular weight distributions using a log-normal distribution model. *Eur. Polym. J.* **2015**, *65*, 197–201.
- (23) van Ruymbeke, E.; Keunings, R.; Bailly, C. Determination of the molecular weight distribution of entangled linear polymers from linear viscoelasticity data. *J. Non-Newtonian Fluid Mech.* **2002**, *105*, 153–175.
- (24) Ansari, M.; Inn, Y. W.; Sukhadia, A. M.; DesLauriers, P. J.; Hatzikiriakos, S. G. Wall slip of HDPEs: Molecular weight and molecular weight distribution effects. *J. Rheol.* **2013**, *57*, 927–948.
- (25) van Ruymbeke, E.; Coppola, S.; Balacca, L.; Righi, S.; Vlassopoulos, D. Decoding the viscoelastic response of polydisperse star/linear polymer blends. *J. Rheol.* **2010**, *54*, 507–538.
- (26) Walsh, D. J.; Zoller, P.Standard Pressure Volume Temperature Data for Polymers; CRC Press, 1995.
- (27) Alexandris, S.; Peponaki, K.; Petropoulou, P.; Sakellariou, G.; Vlassopoulos, D. Linear Viscoelastic Response of Unentangled Polystyrene Bottlebrushes. *Macromolecules* **2020**, *53*, 3923–3932.
- (28) Parisi, D.; Costanzo, S.; Jeong, Y.; Ahn, J. Y.; Chang, T. Y.; Vlassopoulos, D.; Halverson, J. D.; Kremer, K.; Ge, T.; Rubinstein, M.; et al. Nonlinear Shear Rheology of Entangled Polymer Rings. *Macromolecules* **2021**, *54*, 2811–2827.

- (29) van Ruymbeke, E.; Keunings, R.; Stephenne, V.; Hagenaars, A.; Bailly, C. Evaluation of reptation models for predicting the linear viscoelastic properties of entangled linear polymers. *Macromolecules* **2002**, 35, 2689–2699.
- (30) Parisi, D.; Ahn, J.; Chang, T.; Vlassopoulos, D.; Rubinstein, M. Stress Relaxation in Symmetric Ring-Linear Polymer Blends at Low Ring Fractions. *Macromolecules* **2020**, *53*, 1685–1693.
- (31) Likhtman, A. E.; McLeish, T. C. B. Quantitative theory for linear dynamics of linear entangled polymers. *Macromolecules* **2002**, 35, 6332–6343.
- (32) Des Cloizeaux, J. Relaxation and Viscosity Anomaly of Melts Made of Long Entangled Polymers Time-Dependent Reptation. *Macromolecules* **1990**, 23, 4678–4687.
- (33) Tsenoglou, C. Molecular-Weight Polydispersity Effects on the Viscoelasticity of Entangled Linear-Polymers. *Macromolecules* **1991**, 24, 1762–1767.
- (34) Johnston-Hall, G.; Monteiro, M. J. Bimolecular radical termination: New perspectives and insights. *J. Polym. Sci., Part A: Polym. Chem.* **2008**, 46, 3155–3173.
- (35) Johnston-Hall, G.; Monteiro, M. J. Kinetic modeling of "living" and conventional free radical polymerizations of methyl methacrylate in dilute and gel regimes. *Macromolecules* **2007**, *40*, 7171–7179.
- (36) Monteiro, M. J.; de Barbeyrac, J. Free-radical polymerization of styrene in emulsion using a reversible addition-fragmentation chain transfer agent with a low transfer constant: Effect on rate, particle size, and molecular weight. *Macromolecules* **2001**, *34*, 4416–4423.
- (37) Adamy, M.; van Herk, A. M.; Destarac, M.; Monteiro, M. J. Influence of the chemical structure of MADIX agents on the RAFT polymerization of styrene. *Macromolecules* **2003**, *36*, 2293–2301.
- (38) Destarac, M.; Bzducha, W.; Taton, D.; Gauthier-Gillaizeau, I.; Zard, S. Z. Xanthates as chain-transfer agents in controlled radical polymerization (MADIX): Structural effect of the O-alkyl group. *Macromol. Rapid Commun.* **2002**, 23, 1049–1054.
- (39) Destarac, M.; Taton, D.; Zard, S. Z.; Saleh, T.; Six, Y. On the importance of xanthate substituents in the MADIX process. *ACS Sym. Ser.* **2003**, *854*, 536–550.
- (40) Zard, S. Z. The genesis of the reversible radical addition-fragmentation-transfer of thiocarbonylthio derivatives from the Barton-McCombie deoxygenation: A brief account and some mechanistic observations. *Aust. J. Chem.* **2006**, *59*, 663–668.
- (41) Zard, S. Z. Some intriguing mechanistic aspects of the radical chemistry of xanthates. *J. Phys. Org. Chem.* **2012**, *25*, 953–964.
- (42) Destarac, M.; Guinaudeau, A.; Geagea, R.; Mazieres, S.; Van Gramberen, E.; Boutin, C.; Chadel, S.; Wilson, J. Aqueous MADIX/RAFT Polymerization of Diallyldimethylammonium Chloride: Extension to the Synthesis of Poly(DADMAC)-Based Double Hydrophilic Block Copolymers. J. Polym. Sci., Part A: Polym. Chem. 2010, 48, 5163–5171.
- (43) Monteiro, M. J.; Gavrilov, M. Characterization of hetero-block copolymers by the log-normal distribution model. *Polym. Chem.* **2016**, 7, 2992–3002.
- (44) Gavrilov, M.; Monteiro, M. J. Derivation of the molecular weight distributions from size exclusion chromatography. *Eur. Polym. J.* **2015**, *65*, 191–196.
- (45) Rudin, A. Molecular Weight Distributions of Polymers. *J. Chem. Educ.* **1969**, *46*, 595–600.
- (46) Rubinstein, M.; Colby, R. H.Polymer Physics; Oxford, 2003.
- (47) Honerkamp, J.; Weese, J. A Nonlinear Regularization Method for the Calculation of Relaxation Spectra. *Rheol. Acta* **1993**, 32, 65–73.
- (48) Friedman, E. M.; Porter, R. S. Polymer Viscosity-Molecular Weight Distribution Correlations Via Blending for High Molecular-Weight Poly(Dimethyl Siloxanes) and for Polystyrenes. *Trans. Soc. Rheol.* 1975, 19, 493–508.